Available online at www.sciencedirect.com

ScienceDirect

Geochimica et Cosmochimica Acta 229 (2018) 147–161

Geochimica et Cosmochimica Acta

www.elsevier.com/locate/gca

The silicon isotopic composition of fine-grained river sediments and its relation to climate and lithology

G. Bayon [a,b,*], C. Delvigne [b,c], E. Ponzevera [a], A.V. Borges [d], F. Darchambeau [d], P. De Deckker [e], T. Lambert [d], L. Monin [b], S. Toucanne [a], L. André [b]

[a] *IFREMER, Marine Geosciences Unit, F-29280 Plouzané, France*
[b] *Royal Museum for Central Africa, Department of Earth Sciences, B-3080 Tervuren, Belgium*
[c] *CEREGE, Université Aix Marseille, CNRS, IRD, Collège de France, UMS 34, F-13545 Aix-en-Provence Cedex 04, France*
[d] *Chemical Oceanography Unit, Université de Liège, 4000 Liège, Belgium*
[e] *The Australian National University, Research School of Earth Sciences, Canberra ACT 2601, Australia*

Received 8 December 2017; accepted in revised form 13 March 2018; available online 27 March 2018

Abstract

The $\delta^{30}Si$ stable isotopic composition of silicon in soils and fine-grained sediments can provide insights into weathering processes on continents, with important implications on the Si budget of modern and past oceans. To further constrain the factors controlling the distribution of Si isotopes in sediments, we have analysed a large number (n = 50) of separate size-fractions of sediments and suspended particulate materials collected near the mouth of rivers worldwide. This includes some of the world's largest rivers (e.g. Amazon, Congo, Mackenzie, Mississippi, Murray-Darling, Nile, Yangtze) and rivers from the case study areas of the Congo River Basin and Northern Ireland. Silt-size fractions exhibit a mean Si isotopic composition ($\delta^{30}Si = -0.21 \pm 0.19‰$; 2 s.d.) similar to that previously inferred for the upper continental crust. In contrast, clay-size fractions display a much larger range of $\delta^{30}Si$ values from −0.11‰ to −2.16‰, which yield a global $\delta^{30}Si_{clay}$ of $-0.57 \pm 0.60‰$ (2 s.d.) representative of the mean composition of the average weathered continental crust. Overall, these new data show that the Si isotopic signature transported by river clays is controlled by the degree of chemical weathering, as inferred from strong relationships with Al/Si ratios. At a global scale, the clay-bound Si isotopic composition of the world's largest river systems demonstrates a link with climate, defining a general correlation with mean annual temperature (MAT) in corresponding drainage basins. While the distribution of Si isotopes in river sediments also appears to be influenced by the tectonic setting, lithological effects and sediment recycling from former sedimentary cycles, our results pave the way for their use as paleo-weathering and paleo-climate proxies in the sedimentary record.

Keywords: World rivers; Congo basin; Northern Ireland; Si isotopes; Clay minerals; Weathering; Temperature; Precipitation

1. INTRODUCTION

Stable silicon isotopes can be fractionated during Earth surface processes, resulting in a large (about 7‰) range of $\delta^{30}Si$ compositions in the terrestrial environment (e.g. Douthitt, 1982; Ding et al., 1996; André et al., 2006; Poitrasson, 2017). While pristine (unweathered) silicate rocks usually display uniform Si isotopic compositions on continents ($\delta^{30}Si \sim -0.3 \pm 0.2‰$; e.g. Savage et al., 2010, 2012)), their alteration leads to weathering products having very distinctive Si isotopic ratios: a dissolved pool characterized by positive $\delta^{30}Si$ values (up to ∼+4.7‰; e.g. De la

* Corresponding author at: IFREMER, Marine Geosciences Unit, F-29280 Plouzané, France.
E-mail address: gbayon@ifremer.fr (G. Bayon).

https://doi.org/10.1016/j.gca.2018.03.015
0016-7037/

Rocha et al., 2000; Ding et al., 2004, 2011; Georg et al., 2006a; Cardinal et al., 2010; Hughes et al., 2013; Cockerton et al., 2013; Vandevenne et al., 2015; Steinhoefel et al., 2017), and residual clays and iron oxides with negative values (down to $\delta^{30}Si \sim -2.5‰$; e.g. Ziegler et al., 2005a, 2005b; Delstanche et al., 2009; Opfergelt et al., 2010; Steinhoefel et al., 2011; Opfergelt and Delmelle, 2012). This mass-dependent isotopic fractionation mainly results from preferential incorporation of the light ^{28}Si isotope released during silicate weathering into secondary clays and iron oxides, a process that leaves behind an isotopically-heavier dissolved Si fraction in the soil system. On continents, this ^{30}Si-enriched dissolved load is then available for biogeochemical cycling in diatoms and plants within the freshwater watersheds and being ultimately discharged into the oceans (e.g. Frings et al., 2016).

Over the past few years, various relationships have been reported between the degree of Si isotopic fractionation in soils and weathering indices, climate parameters and the age of soils (Ziegler et al., 2005a, 2005b; Cornelis et al., 2010; Opfergelt et al., 2010, 2012; Bern et al., 2010; Pogge von Strandmann et al., 2012; Cornelis et al., 2014). These observations led to the general idea that the $\delta^{30}Si$ composition of fine-grained sediments could be directly related to weathering intensity (Opfergelt and Delmelle, 2012). Despite promising perspectives for reconstructing the evolution of silicate weathering over geological timescales (Delvigne et al., 2016), the usefulness of Si isotopes as weathering proxies is yet to be fully demonstrated. To some extent, this is because most of the above-mentioned literature mainly refers to small-scale investigations of soil sequences or particular river systems, rather than large-scale field studies. In addition, many studies reported $\delta^{30}Si$ data for bulk soils or sediments, hence on samples in which inherited weathering $\delta^{30}Si$ signatures are likely to be obscured by dilution effects due to the presence of quartz or any other primary silicate minerals. For example, investigations of Si isotope systematics in the vast Yangtze and Yellow river basins showed that the variability of $\delta^{30}Si$ in the suspended particulate matter transported along the course of these two rivers was mostly controlled by the relative proportion of clays versus primary silicate minerals in suspended loads (Ding et al., 2004, 2011). This was also the case of one study that reported Si isotopic measurements for various loess and shale samples (Savage et al., 2013). Despite providing unique constraints on the bulk Si isotopic composition of the upper continental crust (UCC), this latter study failed to identify a clear link between $\delta^{30}Si$ in shales and their corresponding degree of weathering intensity, possibly because those fine-grained sedimentary rocks are composed of various amounts of quartz and other primary silicate minerals in addition to secondary clays.

The aim of this study is to further understand the factors controlling the variability of Si isotopic ratios in fine-grained continental sediments. To this purpose, we have analysed an important set of modern river sediments worldwide. A third of these samples comes from some of the world's largest river systems, therefore providing global information on the behaviour of Si isotopes during Earth surface processes. The results obtained on separate clay-size fractions further suggest that $\delta^{30}Si$ is linked to chemical weathering intensity, and identify climate and lithology as important parameters influencing the global distribution of Si isotopes in fine-grained sediments. We also use these data to provide an estimate for the global $\delta^{30}Si$ composition of the weathered upper continental crust.

2. MATERIALS AND METHODS

2.1. Sample collection

Overall, a total of 50 sediments were analysed during this study. Most samples were collected from river watersheds (river bank sediments or suspended particulates), estuaries (tide-dominated environments), or submarine deltas (wave-dominated environments) near the mouth of rivers (Fig. 1; Table 1). In addition, three samples (Congo, Niger, Nile) were collected from more distal locations at continental margins, in deep-sea fan environments. Except for samples from the Congo River tributaries (see below), all river sediments were scooped from recent river bank deposits. The other sediment samples (estuaries, submarine deltas and continental margins) were recovered by coring, and correspond to core-tops or sub-surface sediment layers. Therefore, all studied samples correspond either to modern or relatively recent sediments that have been presumably deposited during the last few centuries.

Selected samples include 17 major river systems draining large (>100,000 km^2) continental areas (e.g. Amazon, Congo, Mississippi, Nile, Niger, Yangtze, Mackenzie, Murray-Darling, Mekong), in addition to other smaller rivers and selected tributaries associated with particular geological settings, such as sedimentary basins (e.g. Adour, Shannon), old cratonic areas from northern South America (e.g. Rio Caura, Caroni and Aro, which are tributaries of the Orinoco River), Western Australia (Gascoyne), and the Fennoscandian Peninsula (Tana), or mantle-derived environments (Pirogues).

Several river sediments ($n = 6$) were also sampled in Northern Ireland (Fig. 2a) from watersheds hosting distinct geological formations (Paleocene basalts, Paleozoic sedimentary rocks, Proterozoic metamorphic rocks). Four of those rivers (River Maine, Six Mile Water, Moyola and Blackwater) discharge into the Lough Neagh, i.e. the largest freshwater lake in the British Isles. The Lower River Bann represents the only river that flows out from the Lough Neagh. These small river basins (<6000 km^2) are characterized by uniform mild and humid (about 1000 mm/yr) climatic conditions.

A series of suspended river particulates ($n = 10$) from the Congo Basin (i.e. the largest river system in Africa) were also analysed (Fig. 2b). This includes 6 samples collected in December 2013 along the Congo River between Kisangani and Kinshasa, and at the confluence point of its largest tributaries (Lualaba, Lindi, Lomani, Aruwimi, Ubangui, Kasai). Four other samples were collected in June 2015 along the Kasai River (the largest left-bank tributary of the Congo River) and its own tributaries (Sankuru, Loange, Kwango). All samples were collected from a small boat using 15-L polyethylene reservoirs. The different Congo

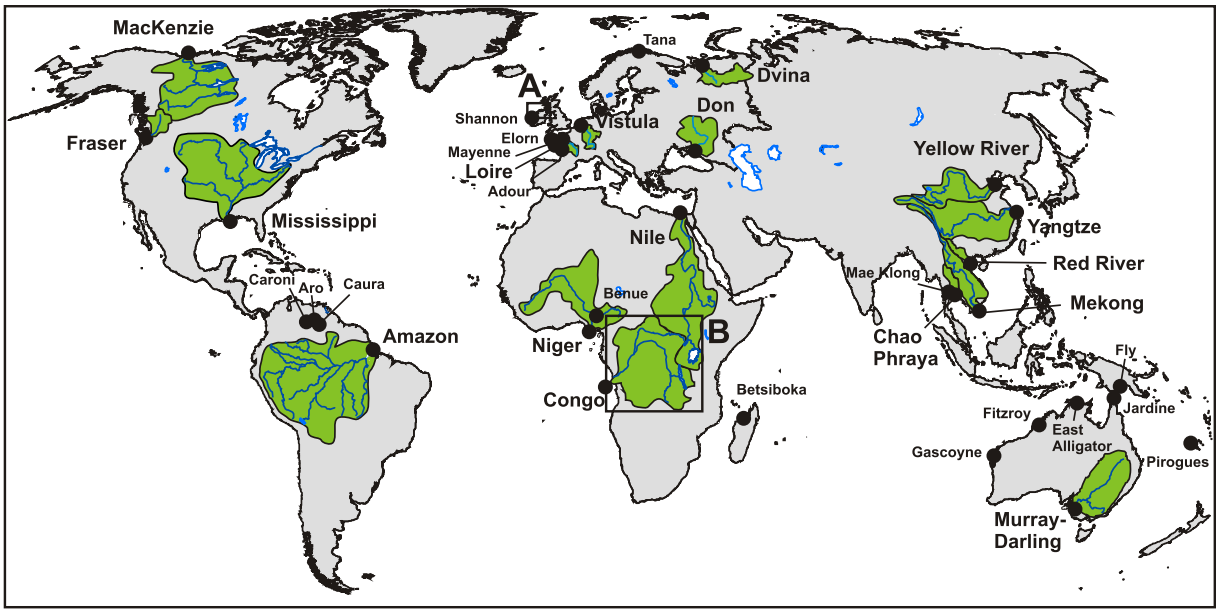

Fig. 1. World map and location of studied river-borne sediments. The green-colored drainage basins correspond to the major river systems with areas >100,000 km^2 investigated during this study (n = 17; excluding tributaries). The boxes refer to the case study areas of Northern Ireland (A) and the Congo River Basin (B) reported in Fig. 2. (For interpretation of the references to colour in this figure legend, the reader is referred to the web version of this article.)

River sub-basins investigated here are characterized by similar tropical climate, with annual rainfall ranging from between 1200 and 1900 mm, but display distinct geological settings. The river catchments draining the northern and eastern margins of the watershed are dominated by Archaean (Ubangui) and Proterozoic (Lualaba, Lindi, Aruwimi) metamorphic basement rocks, while those draining the central and southwestern parts (Lomani, Kasai River and its tributaries) drain mostly Archaean-Early Proterozoic basements, which are masked by extended Mesozoic-Cenozoic sedimentary covers (Fig. 2b).

2.2. Sample and chemical preparations

Details about sample preparation have been reported elsewhere (Bayon et al., 2015). Except for the series of suspended sediment particles from the Congo Basin, other samples were first sieved through a 63 μm mesh to collect the fine-grained fraction. After settlement within the 15 L reservoirs, the Congo River Basin particulates were transferred into 1 L polyethylene bottles, prior to being centrifuged at the laboratory within 50 mL centrifuge tubes and oven dried. All sediment samples (i.e. marine and river sediments, river suspended particulates) were treated using a sequential leaching procedure that quantitatively removes carbonate, Fe-Mn oxyhydroxide and organic components from the bulk (pristine) sediment (Bayon et al., 2002). Clay-size fractions (<4 μm) were then separated from the coarser silt-size fractions (4–63 μm) by centrifuging twice the obtained residual fraction at 1000 and 800 rpm, respectively (Bayon et al., 2015). The reliability of our separation procedure was assessed through repeated granulometric measurements of several sediment samples, including both river and marine sediments. For comparison with δ^{30}Si data for clays, a series of silt-size fractions (n = 9) were also analysed for Si isotopic compositions.

All samples were digested by alkaline fusion following a procedure based on Bayon et al. (2009). About 5 mg of dried sediment powder were transferred into glassy carbon crucibles and placed into an oven at 650 °C for 12 min, after addition of analytical grade NaOH (about 200 mg) and Na_2O_2 pellets (about 50 mg). The obtained melts were dissolved in 50-ml 5% (v/v) sub-boiled HNO_3 to avoid subsequent co-precipitation of any Fe-oxyhydroxide phases, and then stored into centrifuge tubes. Silicon purification was achieved by ion exchange chromatography (AG-50W-X12) based on the procedure developed by Georg et al. (2006b). The procedural Si yield assessed using repeated analyses of reference materials (Diatomite, BHVO-1, SGR-1) gave an average value of 97.3 ± 1.8% (1 s.d.). Total blanks were negligible compared to the amount of samples used in this study.

2.3. Analytical methods

2.3.1. Major elements and clay mineralogy

Major element concentrations for the marine and river-bank sediments used in this study have been already reported elsewhere, together with data for clay mineralogy (Bayon et al., 2015). Clay mineralogical data for Australian river sediments (Murray, West Fitzroy, Gascoyne, East Alligator, Jardine) are from Gingele and De Deckker (2004). Major element concentrations for the clay-size fractions of suspended river particulates from the Congo Basin

Table 1
Si isotopic compositions (‰ NBS28) of clay-size river sediments and corresponding clay mineralogy and climatic parameters.

Sample	Area	Sampling environment	Lat.	Long.	Climatic parameters			Smec	Illi	Kaol	Chlo	Gibb	Verm	Al/Si	Mg/Si	$\delta^{29}Si$	$\delta^{30}Si$
					Zone	MAT	MAP	(%)	(%)	(%)	(%)	(%)	(%)			±2 sd	±2 sd
River	(10^3 km^2)		(°N)	(°E)		(°C)	(mm/yr)										
World rivers																	
Amazon	6300	Sub Delta	3.1	43.4	Tr.W	26.7	2030	59	15	20	6	–	–	0.58	0.003	−0.41 ± 0.06	−0.81 ± 0.02
Congo	3800	Margin	−5.7	11.2	Tr.W	23.9	1520	16	5	79	–	–	–	0.64	0.005	−0.56 ± 0.03	−1.15 ± 0.09
Mississippi	3300	Sub Delta	28.9	89.5	Dry	12.8	760	75	13	12	–	–	–	0.45	0.010	−0.30 ± 0.04	−0.53 ± 0.17
Nile	2900	Margin	32.5	30.4	Dry	26.7	615	73	6	19	<5	–	–	0.47	0.032	−0.39 ± 0.07	−0.74 ± 0.09
Niger	2200	Margin	3.2	6.7	Wa.H	29.4	1140	37	9	54	–	–	–	0.55	0.012	−0.56 ± 0.08	−1.05 ± 0.08
Yangtze	1800	Estuary	31.6	121.0	Te.H	15.6	1270	21	49	11	19	–	–	0.52	0.013	−0.24 ± 0.12	−0.46 ± 0.17
Mackenzie	1800	Sub Delta	69.3	−137.3	SAr	−3.9	380	5	53	21	21	–	–	0.48	0.011	−0.33 ± 0.04	−0.64 ± 0.13
Murray ([A])	1100	River	−35.4	139.2	Dry	18.3	760	24	41	32	–	–	–	0.40	0.006	−0.26 ± 0.06	−0.46 ± 0.11
Benue (* Niger)	1000	River	7.9	6.9	Wa.H	26.6	1080	19	34	32	15	–	–	0.57	0.011	−0.56 ± 0.05	−1.08 ± 0.18
Mekong	800	Delta	11.0	105.1	Wa.H	21.1	1270	<5	20	38	18	–	23	0.69	0.007	−0.40 ± 0.09	−0.77 ± 0.06
Yellow River	750	Delta	37.8	118.9	Dry	12.8	760	49	33	7	12	–	–	0.37	0.020	−0.19 ± 0.09	−0.37 ± 0.09
Don	420	River	47.3	39.1	SAr	6.8	585	73	14	7	5	–	–	0.38	0.011	−0.06 ± 0.12	−0.20 ± 0.18
Northern Dvina	357	Estuary	65.1	39.0	SAr	0.6	740	41	28	16	15	–	–	0.37	0.021	−0.10 ± 0.03	−0.20 ± 0.09
Fraser	230	Sub Delta	49.2	−123.4	SAr	4.4	760	51	19	5	25	–	–	0.34	0.024	−0.08 ± 0.10	−0.11 ± 0.14
Vistula	200	Estuary	54.7	19.3	SAr	7.6	750	<5	60	14	26	–	–	0.36	0.008	−0.11 ± 0.07	−0.26 ± 0.03
Red River	160	Delta	20.3	106.5	Tr.W	24.0	1750	<5	64	14	20	–	–	0.61	0.006	−0.28 ± 0.04	−0.54 ± 0.02
Chao Phraya	160	Delta	13.6	100.6	Tr.W	28.0	1500	55	13	22	10	–	–	0.59	0.007	−0.42 ± 0.10	−0.83 ± 0.17
Loire	120	Estuary	47.3	−1.9	Dry	10.9	750	46	27	19	9	–	–	0.51	0.012	−0.32 ± 0.13	−0.66 ± 0.15
Rio Caroni (* Orinoco)	95	River	8.3	−62.7	Tr.W	25.0	2800	<5	5	66	15	13	–	1.02	0.005	−1.11 ± 0.02	−2.16 ± 0.12
West Fitzroy ([A])	86	River	−17.7	123.6	Dry	19	760	18	36	35	11	–	–	n.a.	n.a.	−0.37 ± 0.04	−0.77 ± 0.03
Gascoyne ([A])	79	River	−29.8	113.8	Dry	22	235	5	41	47	9	–	–	n.a.	n.a.	−0.37 ± 0.12	−0.81 ± 0.12
Fly	76	Sub Delta	−8.7	144.0	Tr.W	26.2	2850	24	35	6	35	–	–	0.56	0.008	−0.38 ± 0.05	−0.71 ± 0.07
Rio Caura (* Orinoco)	47.5	River	7.6	−64.9	Tr.W	25.0	3715	–	5	95	–	–	–	1.01	0.005	−1.14 ± 0.05	−2.15 ± 0.17
Mae Klong	31	River	13.4	100.0	Wa.H	28.0	1200	47	32	21	–	–	–	0.57	0.007	−0.42 ± 0.04	−0.79 ± 0.05
Rio Aro (* Orinoco)	30	River	7.4	−64.0	Tr.W	25.0	3715	n.a.						n.a.	n.a.	−0.79 ± 0.11	−1.58 ± 0.08
Shannon	23	Estuary	52.7	−8.9	Te.H	9.0	1200	13	58	5	23	–	–	0.56	0.009	−0.33 ± 0.03	−0.57 ± 0.12
Adour	16	River	43.5	−1.5	Te.H	13.0	1260	5	55	20	21	–	–	0.60	0.011	−0.26 ± 0.08	−0.57 ± 0.04
Tana	16	River	70.2	28.2	SAr	−2.0	400	n.a.						0.48	0.021	−0.25 ± 0.06	−0.48 ± 0.09
East Alligator ([A])	14	River	−12.4	133.0	Wa.H	27.9	1390	24	15	51	10	–	–	n.a.	n.a.	−0.52 ± 0.02	−1.05 ± 0.03
Betsiboka	11.8	Margin	−15.5	45.7	Wa.H	26.3	1490	n.a.						n.a.	n.a.	−0.63 ± 0.04	−1.29 ± 0.09
Mayenne	4.4	River	47.5	−0.5	Dry	11.8	633	<5	29	29	13	–	30	0.59	0.007	−0.38 ± 0.02	−0.82 ± 0.12
Jardine ([A])	3.3	River	−11.1	142.3	Tr.W	27.1	1845	0	2	89	9	–	–	n.a.	n.a.	−0.88 ± 0.12	−1.73 ± 0.06
Elorn	0.3	Estuary	48.4	−4.4	Te.H	10.8	1120	9	54	18	19	–	–	0.55	0.009	−0.32 ± 0.13	−0.70 ± 0.21
Pirogues	0.1	River	−22.3	166.7	Wa.H	24.8	1200	n.a.						n.a.	n.a.	−0.90 ± 0.08	−1.72 ± 0.09
Northern Ireland rivers																	
Lower River Bann	5.8	River	54.9	−6.5	Te.H	8.7	1000	64	10	16	10	–	–	0.54	0.007	−0.34 ± 0.05	−0.65 ± 0.11
River Foyle	2.9	River	54.8	−7.5	Te.H	8.7	1110	–	59	–	41	–	–	0.40	0.007	−0.09 ± 0.06	−0.25 ± 0.06
Blackwater	1.1	River	54.5	−6.6	Te.H	8.7	1000	19	16	19	46	–	–	0.55	0.007	−0.24 ± 0.07	−0.46 ± 0.10
Moyola	0.3	River	54.8	−6.5	Te.H	8.7	1110	14	37	25	24	–	–	0.51	0.010	−0.22 ± 0.08	−0.45 ± 0.06

River Maine	0.3	River	54.7	−6.3	Te.H	8.7	1000	98	–	<5	–	0.53	0.019	−0.65 ± 0.14	−1.20 ± 0.16
Six Mile Water	0.3	RIver	54.7	−6.1	Te.H	8.7	1000	82	<5	<5	13	0.48	0.016	−0.48 ± 0.06	−0.92 ± 0.09
Congo Basin rivers															
Lualaba	1035	River	0.6	24.8	Wa.H	22.2	1260	n.a.				0.87	0.003	−0.82 ± 0.05	−1.59 ± 0.10
Kasai (downstream)	890	River	−3.2	16.2	Wa.H	23.5	1500	n.a.				0.81	0.001	−0.58 ± 0.05	−1.16 ± 0.03
Ubangui	640	River	−0.5	17.7	Tr.W	25.1	1640	n.a.				0.95	0.001	−0.84 ± 0.07	−1.64 ± 0.16
Kasai (upstream)	245	River	−4.4	20.6	Wa.H	23.8	1485	n.a.				0.95	0.001	−0.71 ± 0.01	−1.43 ± 0.11
Sankuru	148	River	−4.3	20.4	Tr.W	24.4	1590	n.a.				0.80	0.002	−0.62 ± 0.04	−1.21 ± 0.07
Kwango	176	River	−3.4	17.3	Wa.H	21.8	1310	n.a.				0.69	0.003	−0.47 ± 0.04	−0.93 ± 0.09
Aruwimi	122	River	1.2	23.6	Tr.W	24.7	1770	n.a.				0.91	0.001	−0.83 ± 0.04	−1.66 ± 0.07
Lomani	116	River	0.8	24.3	Wa.H	24.2	1350	n.a.				0.66	0.001	−0.46 ± 0.16	−0.94 ± 0.07
Loange	42	River	−4.3	20.0	Tr.W	24.1	1620	n.a.				0.99	0.002	−0.68 ± 0.07	−1.34 ± 0.09
Lindi	39	River	0.6	25.1	Tr.W	24.6	1855	n.a.				0.97	0.001	−0.84 ± 0.03	−1.61 ± 0.01

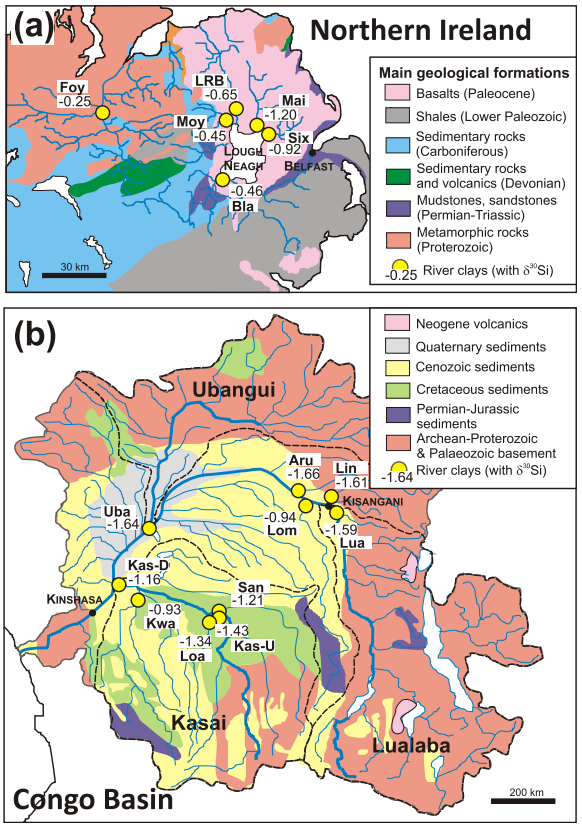

Fig. 2. Simplified lithological maps of Northern Ireland (a) and the Congo River Basin (b) areas, with position of studied river bank sediments (Northern Ireland) or suspended particulate (Congo Basin) samples (yellow circles), with corresponding $\delta^{30}Si$ compositions for clay-size detrital fractions. Northern Ireland: Foy (River Foyle); Mo (Moyola River); LRB (Lower River Bann); Mai (River Maine); Six (Six Mile Water) and Bla (River Blackwater). Congo Basin: Uba (Ubangui River); Kas-D (River Kasai, downstream); Kwa (Kwango River); Loa (Loange River); Kas-U (River Kasai, upstream); San (Sankuru River); Lom (Lomani River); Aru (Aruwimi River); Lin (Lindi River) and Lua (Lualaba River, or Upper Congo). (For interpretation of the references to colour in this figure legend, the reader is referred to the web version of this article.)

were determined by ICP-AES at the Royal Museum for Central Africa after lithium metaborate fusion, with average accuracies typically below 5%.

2.3.2. Silicon isotopic measurements

Silicon isotopic compositions were measured with a Neptune MC-ICPMS at the Pôle Spectrométrie Océan (Brest), using an APEX desolvation unit and a medium mass resolution mode. Mass bias correction was achieved by Mg external doping, with a resulting [Si]/[Mg] ratio of ~1. Measured $^{30}Si/^{28}Si$ and $^{29}Si/^{28}Si$ ratios corrected from blank contribution and mass discrimination were normalized to the conventional NBS28 reference standard using a sample-standard bracketing method. Three reference materials (Diatomite, BHVO-1, SGR-1) were also repeatedly analyzed during the course of this study (from June 2015 to July 2016) in order to assess the accuracy and

Table 2
Si isotopic compositions (‰) of reference materials and Loire River sediments.

Sample	$\delta^{29}Si$ ±2 sd	$\delta^{30}Si$ ±2 sd
BHVO-1		
Jun-2015	−0.15 ± 0.03	−0.30 ± 0.10
Jan-2016	−0.10 ± 0.04	−0.20 ± 0.07
Apr-2016	−0.14 ± 0.03	−0.26 ± 0.02
Jul-2016	−0.16 ± 0.21	−0.31 ± 0.06
Mean	**−0.14 ± 0.06**	**−0.27 ± 0.10**
Reference[*]	*−0.2 ± 0*	*−0.3 ± 0.05*
Diatomite		
Jun-2015	0.67 ± 0.07	1.27 ± 0.06
Jan-2016	0.67 ± 0.02	1.32 ± 0.11
Apr-2016	0.65 ± 0.05	1.27 ± 0.06
Jul-2016	0.62 ± 0.18	1.27 ± 0.05
Mean	**0.65 ± 0.05**	**1.28 ± 0.05**
Reference[**]	*0.64 ± 0.1*	*1.26 ± 0.20*
SGR-1		
Jun-2015	0.03 ± 0.12	0.03 ± 0.15
Jan-2016	0.04 ± 0.07	0.08 ± 0.09
Apr-2016	0.04 ± 0.07	0.08 ± 0.24
Jul-2016	0.02 ± 0.20	0.08 ± 0.25
Mean	**0.03 ± 0.02**	**0.07 ± 0.05**
Reference[***]	*0.01 ± 0.1*	*0.03 ± 0.12*
Loire River sediments		
Port-Lavigne	−0.25 ± 0.19	−0.57 ± 0.08
Donges	−0.36 ± 0.08	−0.69 ± 0.12
Cordemais	−0.35 ± 0.04	−0.72 ± 0.03
Mean	**−0.32 ± 0.13**	**−0.66 ± 0.15**

Reported values correspond to the average of 3 distinct analyses.
Reference values:
[*] Abraham et al. (2008).
[**] Reynolds et al. (2007).
[***] Hughes et al. (2011).

reproducibility of measured NBS28-normalized $\delta^{29}Si$ and $\delta^{30}Si$ values. The obtained values agree well with those reported earlier in previous studies (Table 2). During each analytical session, three distinct analyses were performed for every studied sample and reference materials, and reported Si isotopic compositions correspond to average values of these 3 analyses ± associated standard deviation (2 s.d.). In addition, a series of 3 sediment samples (clay-size fractions) from the Loire River (France) was used to assess both sample representativeness and the analytical uncertainty associated with sediment preparation. These samples were collected along a 50-km transect along the river estuary. The obtained uncertainties (2 s.d.) on the average $\delta^{29}Si$ (−0.32‰) and $\delta^{30}Si$ (−0.66‰) values associated with sediment sampling and preparation were ±0.13‰ and 0.15‰, respectively (Table 2). All Si isotopic data reported in this study fall on a well-defined mass-dependent fractionation array on a $\delta^{29}Si$ versus $\delta^{30}Si$ plot, with a slope of ~0.512.

3. RESULTS

Results for NBS28-normalized Si isotopic ratios are listed in Table 1 (clay-size fractions) and Table 3 (silt-size fractions). Table 1 also includes previously published clay mineralogical data (Bayon et al., 2015; Gingele and De Deckker, 2004) and information on climatic parameters in corresponding river basins. Note that the mean annual air temperature (MAT) and precipitation (MAP) data for each river system listed in Table 1 are derived from Bayon et al. (2016) or from the CLIMWAT climatic database managed by the Food and Agriculture Organization of the United Nations (FAO).

Table 3
Si isotopic compositions (‰) of silt-size river sediments.

Sample River	Al/Si	$\delta^{29}Si$ ±2 sd	$\delta^{30}Si$ ±2 sd
World rivers			
Amazon	0.32	−0.16 ± 0.02	−0.29 ± 0.16
Yangtze	0.27	−0.09 ± 0.11	−0.25 ± 0.18
MacKenzie	0.23	−0.18 ± 0.12	−0.33 ± 0.08
Mekong	0.14	−0.07 ± 0.07	−0.15 ± 0.22
Yellow River	0.17	−0.02 ± 0.03	−0.06 ± 0.06
Northern Dvina	0.30	−0.05 ± 0.09	−0.14 ± 0.22
Red River	0.24	−0.12 ± 0.11	−0.26 ± 0.14
River Foyle	0.24	−0.04 ± 0.05	−0.05 ± 0.26
Rio Caura	0.44	−0.21 ± 0.06	−0.43 ± 0.13

Silt-size sediments exhibit a narrow range of Si isotopic compositions, from $\delta^{30}Si$ −0.05‰ (River Foyle) to −0.43‰ (Rio Caura). This last sample is significantly depleted in ^{30}Si compared to the other studied silt fractions, possibly due to partial contamination by clays during our grain-size separation procedure. In contrast, clay-size fractions display Si isotopic compositions ($\delta^{30}Si_{clay}$) from −0.11‰ (Fraser) to −2.16‰ (Rio Caura and Rio Caroni), which almost encompass the full range of $\delta^{30}Si$ data reported in the literature for bulk soils and clays (between about −2.95 and −0.16‰; Opfergelt and Delmelle, 2012; Frings et al., 2016). Many samples investigated during this study were collected in the marine environment, hence with the possibility that they could include some authigenic clays formed by early diagenetic processes (e.g. reverse weathering; Michalopoulos and Aller, 1995). While the presence of neoformed clay minerals in some particular samples cannot be fully excluded, evidence that the marine sediments recovered in the deep-sea fan environments at the Congo (−1.15‰) and Niger (−1.05‰) margins display very similar Si isotopic compositions than corresponding $\delta^{30}Si_{clay}$ signatures of river sediments from their main tributary (Kasai River: −1.16‰ and Benue River: −1.08‰, respectively) suggests that this potential effect can be probably neglected in this study.

4. DISCUSSION

4.1. The Si isotopic composition of the unweathered and weathered upper continental crust

The silt-size fraction of river sediments can provide integrated information on the geochemical composition of the pristine, or unweathered, source rocks in corresponding watersheds. As shown recently using major element concentrations, silt-size separate fractions from major river sys-

tems worldwide display mean geochemical signatures similar to global reference estimates for the UCC, loess and continental-scale reference values for soils (Bayon et al., 2015). Similarly, the average value obtained for neodymium (Nd) isotopic ratios for the same silt-size fractions was found to match very well with previous global estimates inferred from the analyses of river particulates and loess deposits worldwide (Bayon et al., 2015). In this study, considering only the data obtained for sediments from major river systems (i.e. Amazon, Yangtze, Mackenzie, Mekong, Yellow River, Northern Dvina, Red River), the obtained mean $\delta^{30}Si$ composition for silt-size fractions of world river sediments is fixed at $-0.21 \pm 0.19‰$ (2 s.d; n = 7). This value coincides well with the estimate for the average Si isotopic composition of the upper continental crust ($-0.25 \pm 0.16‰$; Savage et al., 2013).

Taken together, the cumulative area of the major river basins investigated in this study with watersheds larger than >100,000 km^2 (n = 17; excluding the Benue River, i.e. a tributary of the Niger River) accounts for a total of 26.4 $\times 10^6$ km^2, hence representing about 25% of the entire continental area that drains into the global ocean (105×10^6 km^2; Milliman and Farnsworth, 2011). In terms of sediment discharge, these rivers export altogether about 2.7 Gt of suspended particles each year, which represents about 15% of the annual sediment flux to the global ocean (about 18 Gt/yr; Milliman and Syvitski, 1992). This relatively large coverage area and associated sediment flux indicates that the results reported here for clay-size fractions ($\delta^{30}Si_{clay}$) can be used to provide a first global estimate for the Si isotopic composition of the average weathered upper continental crust, yielding $\delta^{30}Si_{clay} = -0.57 \pm 0.60‰$ (2 s.d.). Note that this value does not correspond to an area-weighted or a flux-weighted average value. Below, we discuss the processes that account for the large dispersion of $\delta^{30}Si$ values measured in the clay-size fractions of river sediments worldwide, with particular emphasis on the role of chemical weathering, climate and lithology.

4.2. Silicon isotopic fractionation during weathering

A strong correlation ($R^2 = 0.80$) is observed between the Si isotopic composition of our clay-size fractions ($\delta^{30}Si_{clay}$) and corresponding Al/Si ratios in clays (Fig. 3a). This global relationship echoes with that reported earlier between Si isotopes and the chemical index of alteration (CIA) in bulk soils from Guadeloupe, Cameroon, Iceland, Hawaii and Puerto Rico (Opfergelt and Delmelle, 2012), hence further suggesting that the $\delta^{30}Si$ signature of weathered sedimentary products is related to chemical weathering intensity. These relationships confirm that the distribution of Si isotopes in weathering products is related to desilication, i.e. the process by which alteration of silicate minerals is accompanied by formation of secondary clays with higher Al/Si ratios (due to net Si loss). In contrast, measured $\delta^{30}Si_{clay}$ compositions display a negative correlation with corresponding Mg/Si ratios (Fig. 3b), reflecting the fact that Mg is highly mobile during weathering processes and typically depleted in soils relative to Si. However, compared to Al/Si, the more scattered distribution of studied river samples in the Mg/Si versus $\delta^{30}Si_{clay}$ plot is probably best explained by lithological effects, in particular those related to preferential weathering of Mg-rich mafic igneous rocks.

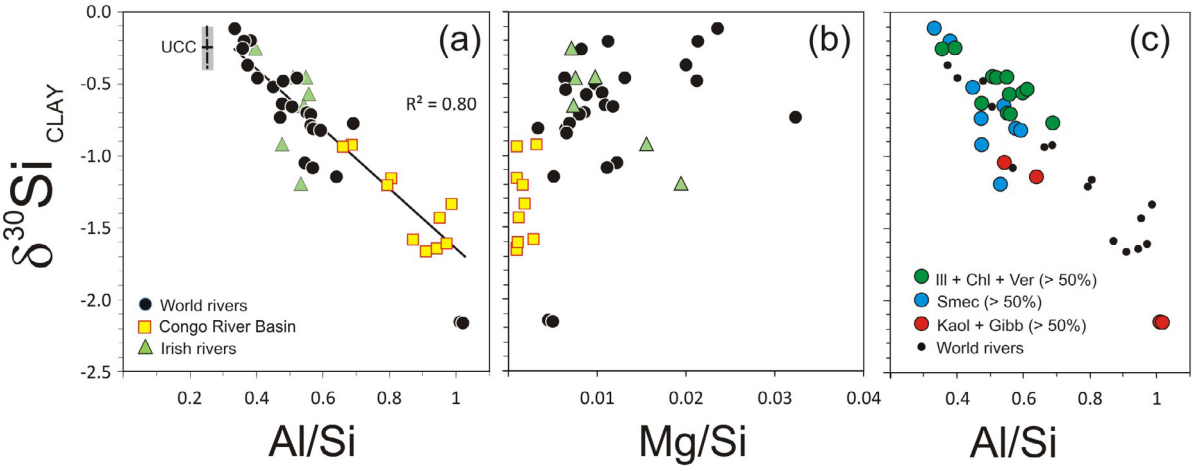

Fig. 3. Relationships between the Si isotopic composition of river clay-size fractions ($\delta^{30}Si_{clay}$) and corresponding (a) Al/Si ratios; (b) Mg/Si ratios; and (c) Al/Si ratios and clay mineralogy. Reported are data for riverbank samples from Northern Ireland (green triangles), river suspended particulates from the Congo Basin (yellow squares), and other river-borne sediments worldwide analysed during this study (black circles). (a) The dashed lines and associated grey bands correspond to the mean values (and associated uncertainties) for the average upper continental crust composition, as inferred from Si isotopic compositions of loess and shale samples ($\delta^{30}Si = -0.25 \pm 0.16‰$; Savage et al., 2013) and Al/Si ratios of global UCC estimates (see Rudnick and Gao, 2003, and references therein). Also shown are the best-fit linear trends (black lines) for all samples (n = 50) and associated coefficient of regressions (R^2). (c) Symbols: (green circles) River sediment samples dominated by illite-chlorite-vermiculite assemblages (>50% of the total clay mineral assemblage). River sediment samples with at least 50% of smectite and kaolinite-gibbsite clay mineral contents (blue and red circles, respectively). (For interpretation of the references to colour in this figure legend, the reader is referred to the web version of this article.)

The degree of soil desilication is time-dependent, and earlier findings have linked the progressive ^{30}Si-depletion in soils of increasing age with repeated cycles of clay dissolution/precipitation (Bern et al., 2010; Cornelis et al., 2014). In this study, the observed relationship between $\delta^{30}Si_{clay}$ and Al/Si in river sediments is also coherent with recent theoretical studies, which emphasized the importance of major element chemical composition in controlling silicon isotopic fractionation during mineral formation (Méheut and Schauble, 2014). As shown in that latter study, the degree of Si isotopic fractionation is strongly dependent on the incorporation of Al and other major cations within the structure of silicate minerals, with lighter Si isotopes being preferentially partitioned into mineral phases with high Al/Si and Mg/Si ratios. Experimental investigations have also led to the suggestion that Si isotopic fractionation during adsorption onto mineral surfaces could occur in presence of substantial amounts of Al in the parental fluid, with higher Al concentrations leading to larger Si isotopic fractionation (Oelze et al., 2014, 2015). Increasing amounts of Al in soil solutions would drive faster Si removal during clay formation, resulting in a stronger kinetic isotopic fractionation (Oelze et al., 2015). While this effect is unlikely to play a major role in environments with near-neutral pH conditions, the increasing solubility of most dissolved Al species ($Al(OH)_2$, $AlOH^{2+}$, Al^{3+}) in acidic freshwaters (pH < 5) could possibly result, at least locally, in secondary clays characterized by strong δ^{30}Si depletion. In this study, such acidic conditions are prevalent in the so-called 'black' rivers that drain the Guiana Shield in northern South America (Edmond et al., 1995). This would agree well with the fact that the most ^{30}Si-depleted signatures encountered in this study ($\delta^{30}Si_{clay} \sim -2.15‰$) correspond to samples collected from the same 'black' rivers in Venezuela (Rio Caroni and Rio Caura). Alternatively, the highly depleted $\delta^{30}Si_{clay}$ values associated with Venezuelan rivers could also simply reflect the presence of very intense weathering processes in the plateaus of the Guiana Highlands.

Interestingly, as shown in Fig. 3a, the intersect of the best-fit trend observed for the above-mentioned relationship with the average δ^{30}Si composition of the pristine (unweathered) upper continental crust ($-0.25 \pm 0.16‰$; Savage et al., 2013) gives an Al/Si value of about 0.35, hence substantially higher than previous estimates for the average Al/Si composition of the UCC (0.25 ± 0.01; see Rudnick and Gao, 2003 and references therein). In agreement with a recent study (Ameijeiras-Mariño et al., 2017), the observed mismatch between $\delta^{30}Si_{clay}$ and Al/Si ratios could suggest that clay mineral formation in environments characterized by very low silicate weathering rates (or during the early stages of chemical weathering in soils), such as those encountered under cold and/or arid climatic conditions for example, is not accompanied by significant Si isotopic fractionation. While further studies would be needed to confirm this hypothesis, this would be coherent with recent experimental works, which argued that slow kinetic precipitation of secondary minerals could lead to products having a δ^{30}Si composition similar to that of their parental fluid solutions, hence without any measurable Si isotopic fractionation (Oelze et al., 2014, 2015). Alternatively, as discussed in another recent study (Opfergelt et al., 2017), another possible explanation accounting for the mismatch between Al/Si and $\delta^{30}Si_{clay}$ in cold environments could relate locally to the presence of organic-rich peatlands, which typically form under waterlogged anoxic conditions in cool climatic regions. In such anoxic environments, Si concentration in soil solutions can reach supersaturation with respect to amorphous silica, due to formation of Al-organic complexes, hence leading to preferential incorporation of lighter Si isotopes and, as a consequence, to heavier δ^{30}Si compositions in soil solutions. As a consequence, precipitation of secondary clay minerals from enriched δ^{30}Si soil solutions could also possibly account, at least partly, for the relatively heavy δ^{30}Si clay compositions observed in particular cool climatic environments.

Clay mineralogy is also thought to play an important role in controlling the distribution of Si isotopic ratios in soils (e.g. Opfergelt et al., 2010). Previous investigations reporting coupled analyses of both clays and corresponding parent rocks have shown that distinct clay minerals are tagged with specific δ^{30}Si signatures, and this has been interpreted in terms of different degree of isotopic fractionation. So far, however, the degree of Si isotopic fractionation between secondary clays and silicate rocks has only been reported for a few minerals, including smectite (with $\Delta^{30}Si_{clay\text{-}parent\ silicate\ material}$ ranging from ~0 to −1.5‰; Georg et al., 2007, 2009; Opfergelt et al., 2010), allophane (−1.8‰; Ziegler et al., 2005b) and kaolinite (from −1.6‰ to −2‰; Ziegler et al., 2005b; Méheut et al., 2007). Additional field-based, theoretical and/or experimental studies will be needed to determine fractionation factors associated with other clay minerals, especially those such as illite and chlorite that are encountered preferentially in poorly weathered environments. In this study, for any given range of Al/Si ratios, the samples dominated by illite-chlorite-vermiculite assemblages (i.e. accounting for >50% of the total clay fraction) generally display heavier isotopic compositions than smectite- and kaolinite-rich samples (Fig. 3c). When considering paired clay- and silt-size δ^{30}Si data for samples characterized by very high illite-chlorite contents (>80% of the total clay fraction; i.e. River Foyle, and Red River) and assuming that the Si isotopic composition of corresponding silt-size fractions is representative of the parental rock signature, the calculated $\Delta^{30}Si_{clay\text{-}parent\ silicate\ material}$ values for illite-chlorite range between −0.21 to −0.28‰. Presumably, these low $\Delta^{30}Si_{clay\text{-}parent\ silicate\ material}$ values could reflect a lower degree of Si isotopic fractionation for illite and chlorite during weathering processes in soils, relative to smectite or kaolinite. Another possible explanation would be that the low δ^{30}Si signatures characteristic of illite-chlorite and smectites assemblages in river sediments partly reflect the presence of inherited (recycled) clay minerals associated with erosion of low-grade metamorphic and/or hydrothermally-altered rocks in river basins. Indeed, as predicted by theoretical work (Méheut et al., 2007, 2009), the degree of Si isotopic fractionation during mineral formation strongly decreases with increasing temperatures, so that illite and chlorite formed at relatively high temperature (40–400 °C) during the low-grade metamorphism

and/or the hydrothermal alteration of magmatic bodies would be expected to display relatively low $\delta^{30}Si$ values, close to the average isotopic compositions of unweathered crystalline continental crust ($-0.22 \pm 0.07‰$, Savage et al., 2013). The presence of such pre-formed clays derived from the erosion of metamorphic or hydrothermally-altered rocks could also possibly explain the discrepancy observed between Al/Si and $\delta^{30}Si$ values in the upper left-hand side of Fig. 3a (see discussion above). In any case, the above consideration suggests that the distribution of $\delta^{30}Si$ values in fine-grained river sediments partly reflects, in addition to soil desilication processes, the fact that clay mineral assemblages transported by large river systems correspond to various mixtures between poorly ^{30}Si-fractionated (heavier) clays (illite, chlorite) and more ^{30}Si-depleted (lighter) minerals, such as smectite and/or kaolinite.

4.3. Global relationships between river $\delta^{30}Si_{clay}$ and climate

In addition to chemical weathering, the potential link between Si isotopes and climate was examined by plotting $\delta^{30}Si_{clay}$ against modern climatic parameters for corresponding drainage basins (Table 1; Fig. 4). The Si isotopic compositions of clay-size fractions display weak but overall general correlations with mean annual temperatures (MAT) and precipitations (MAP). The strong dependency of silicate weathering rates on temperature and precipitation in watersheds has been well documented in many experimental and field-based investigations of weathering (e.g. White and Blum, 1995; White et al., 1999; Dessert et al., 2003). As will be discussed below (Section 4.4), some of the observed Si isotopic variability in river sediments can be ascribed to lithological effects, in particular for those samples derived from watersheds draining particular geological settings. In addition, recycling of fine-grained sediments issued from former sedimentary cycles is also likely to obscure any relationship between measured $\delta^{30}Si$ clay signatures and modern climatic condition (Section 4.4.2). However, when considering only the world's largest rivers with basin areas >100,000 km^2 (except for the particular Mackenzie River; see below), the Si isotopic composition of clays defines a good correlation with temperature ($R^2 = 0.73$; n = 16; Fig. 5), which follows the general logarithmic equation: $\delta^{30}Si_{clay} = Ln(0.858–0.016 \times MAT)$.

The global relationship between Si isotopes and climate is also illustrated by reporting measured $\delta^{30}Si_{clay}$ values according to distinct climatic zones defined using arbitrary temperature and rainfall conditions, and against Al/Si ratios (Table 1; Fig. 6). Average $\delta^{30}Si_{clay}$ compositions for each climate zone are reported in Table 4. The obtained $\delta^{30}Si_{clay}$ estimates show a clear climate-dependency from cold and dry subarctic environments (mean $\delta^{30}Si_{clay} = -0.32 \pm 0.20‰$; n = 6) to warm and wet tropical climate regions (mean $\delta^{30}Si_{clay} = -1.37 \pm 0.51‰$; n = 14). In addition, the distinction of each climatic zones in the $\delta^{30}Si_{clay}$ versus Al/Si relationship discussed above (Section 4.2) also

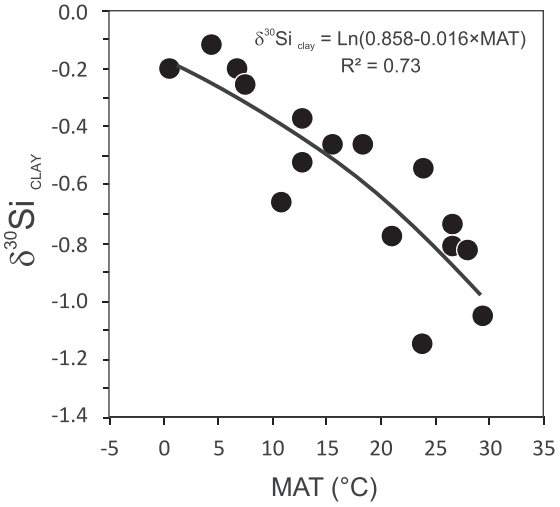

Fig. 5. The general relationship between $\delta^{30}Si_{clay}$ and temperature (°C) in major river systems. The obtained best-fit trend (logarithmic equation) and associated coefficient of regression (R^2) includes all studied watersheds with drainage area >100,000 km^2, excluding the Benue River and Mackenzie River. See text for details.

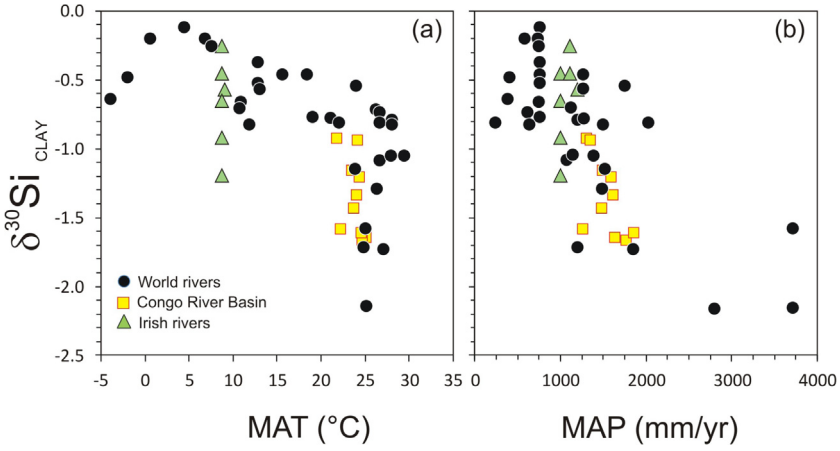

Fig. 4. Relationships between river $\delta^{30}Si_{clay}$ and climate. All reported data are from this study. The climatic parameters used for comparison include (a) the mean annual temperatures (MAT; °C); and (b) mean annual precipitation (MAP; mm) in corresponding drainage basins. Symbols: see Fig. 4 caption.

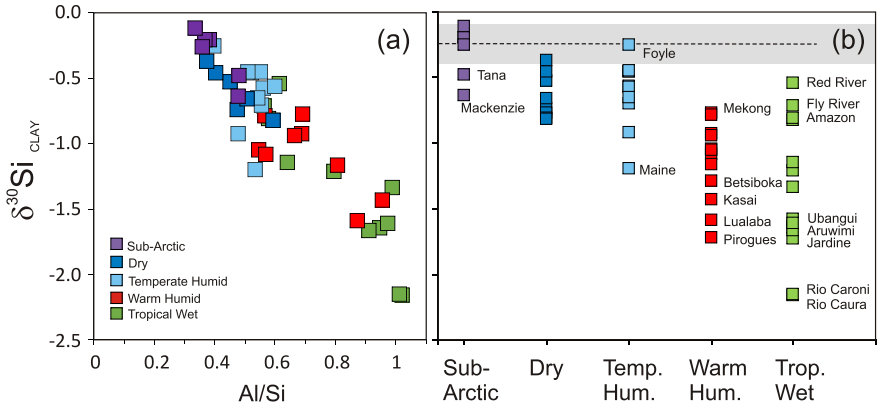

Fig. 6. Relationship between climate and Si isotopic ratios in clay-size fractions of world river sediments. Studied samples are classified into five different climatic zones, defined according to the following arbitrary criteria: (1) 'Sub-Arctic': cold and dry regions, with MAT < 8 °C and MAP < 800 mm; (2) 'Dry': Temperate and warm dry environments, with MAT > 10 °C and MAP < 800 mm; (3) 'Temp. Hum.': Temperate and humid regions, with 8 °C < MAT < 16 °C and MAP > 1000 mm; (4) 'Warm Hum.': Tropical regions with humid conditions, with MAT > 20 °C and MAP < 1500 mm; and (5) 'Trop. Wet': Tropical wet regions, with MAT > 20 °C and MAP > 1500 mm.

Table 4
Average $\delta^{30}Si$ clay values for climatic zones.

	Climatic zones	MAT °C	MAP mm	$\delta^{30}Si$ (±1 sd)	N
Sub-arctic	Cold & dry environments	<8	<800	−0.32 ± 0.20	6
Dry	Temperate/warm & dry	>10	<800	−0.64 ± 0.17	8
Temp. Hum.	Temperate & humid	>8 < 16	>1000	−0.62 ± 0.27	10
Warm Hum.	Warm & humid	>20	<1500	−0.83 ± 0.30	12
Trop. Wet	Tropical & wet	>20	>1500	−1.37 ± 0.51	14

The list of studied river sediments and corresponding climatic zone is given in Table 1.

clearly supports the global link between climate, soil desilication, clay mineralogy and Si isotopic composition (Fig. 6a).

Of course, the large dispersion of $\delta^{30}Si_{clay}$ values observed in Figs. 4 and 6 indicates that other variables also control the overall distribution of Si isotopes in fine-grained sediments. For example, while most subarctic rivers display $\delta^{30}Si_{clay}$ similar to the average UCC composition, indicative of limited weathering conditions, sediments from the Mackenzie and Tana rivers exhibit significantly lighter $\delta^{30}Si_{clay}$ values (−0.68‰ and −0.48‰, respectively; Fig. 6b). These high-latitude rivers drain permafrost-dominated watersheds characterized by negative MAT (<−2°C). In this context, the observed ^{30}Si-depleted isotopic signatures could indicate that particular weathering processes are at play in permafrost-dominated regions, associated with larger isotopic fractionation at very low temperature conditions (Pokrovsky et al., 2013; Opfergelt et al., 2017). Another possible explanation would also be that these relatively depleted $\delta^{30}Si$ signatures for clay-size fractions from the Mackenzie and Tana rivers indicate recycling of older sediments formed during previous weathering cycles. This issue will be discussed in details below when discussing the case-study of the Congo Basin (Section 4.4.2).

In addition to climate, tectonics and relief also play fundamental roles in erosion and weathering processes on continents (e.g. Edmond and Huh, 1997; Gaillardet et al., 1999a; West et al., 2005). High mountain regions are typically associated with kinetically-limited weathering regimes due to high rates of mechanical erosion, which ultimately lead to export of poorly weathered material by rivers. In contrast, lowlands and high plateau areas generally correspond to transport-limited weathering regimes, characterized by the presence of thick strongly weathered soils but low chemical weathering rates. In Fig. 6, the samples exhibiting the heaviest $\delta^{30}Si_{clay}$ values in tropical humid/wet climate regions correspond to river basins that drain high and young mountain ranges. This is the case for example of the Mekong River ($\delta^{30}Si_{clay} = -0.77‰$; with a maximum elevation of ~5100 m), Red River (−0.54‰; 3100 m), Fly River (−0.71‰; 4000 m) and the Amazon (−0.81‰; 5500 m). In contrast, the river sediments exhibiting the lightest $\delta^{30}Si$ signatures are encountered in tropical flat plains such as the Jardine River ($\delta^{30}Si_{clay} = -1.73‰$; 164 m), or in the relatively flat high plateaus associated with the old cratonic areas drained by the Betsiboka in Madagascar (−1.29‰) and the Orinoco (down to −2.16‰) and Congo (down to −1.66‰) river tributaries. Taken together, the above observations suggest that the inverse relationship between erosion rates and the degree of chemical weathering accounts, at least to some extent, for some of the observed $\delta^{30}Si_{clay}$ variability in world river sediments.

4.4. Lithological controls on the distribution of $\delta^{30}Si_{clay}$ in river sediments

We now consider the results obtained for the series of sediments and suspended particulates from rivers of Northern Ireland and the Congo Basin. Because both settings are characterized by relatively uniform climate conditions, these two case studies are particularly well-suited for investigating separately the role of lithology in controlling the distribution of Si isotopes in fine-grained sediments.

4.4.1. Rivers of Northern Ireland

The rivers of Northern Ireland drain watersheds characterized by distinct geological settings. The British Tertiary Volcanic province that outcrops in the northeastern part of the region is bordered on the south by Lower Paleozoic shales and on the west by old Proterozoic metamorphic terranes. At present, the entire area is mainly covered by glacial tills left behind the retreat of the British-Irish ice-sheet during the last deglaciation period (e.g. Dempster et al., 2013). A substantial fraction of the fine-grained particles transported by Northern Irish rivers is expected to derive from erosion of late glacial deposits and/or post-glacial soil sequences that developed after ca. ~16 kyr BP above till deposits. To a first approximation, we can consider that NE Irish soils probably have a roughly similar age, and hence that measured $\delta^{30}Si_{clay}$ differences between each of the studied watersheds mostly result from lithological effects.

The role of lithology was investigated by plotting $\delta^{30}Si$ versus the proportion of smectite minerals (i.e. a product of basalt weathering) and the neodymium (Nd) isotopic composition of the same clay-size sediment fractions, as reported in Bayon et al. (2015). In contrast to Si, Nd isotopes (expressed from hereafter using the conventional ε_{Nd} notation) are not decoupled during weathering processes and hence can be used as provenance tracers (Goldstein and Hemming, 2003). In the case of Northern Irish rivers, high smectite contents and radiogenic (high) ε_{Nd} values characterize clays derived from the British Tertiary Volcanic province, whereas river material transported from the Paleozoic and Proterozoic terranes display much lower smectite contents and ε_{Nd} compositions (Bayon et al., 2015). In Fig. 7, $\delta^{30}Si_{clay}$ define strong correlations with both smectite contents and ε_{Nd} values. This finding suggests that the Si isotopic variability displayed by NE Irish river sediments is controlled to a large extent by sediment mixing between: (1) clays derived from basaltic soils (with $\delta^{30}Si_{clay} \sim -1.20‰$; $\varepsilon_{Nd} \sim +1$ and smectite ~100%); and (2) clays derived from metamorphic/sedimentary terranes (with $\delta^{30}Si_{clay} \sim -0.25‰$; $\varepsilon_{Nd} \sim -16$; smectite ~0%) dominated by illite-chlorite clay mineral assemblages possibly inherited from regional metamorphic rocks, which maintain the isotopic signatures close to the UCC. Because all soils in NE Ireland are presumed to be of similar age, integrating ongoing weathering processes since the end of the last glacial period (e.g. about 16 kyr ago), the marked $\delta^{30}Si$ (~1‰) difference observed between the two type of clays (smectite and illite-chlorite) is best explained by the fact that basaltic rocks weather much faster and more intensively than old metamorphic basement rocks, hence leading to formation of secondary clays characterized by more depleted $\delta^{30}Si_{clay}$ values.

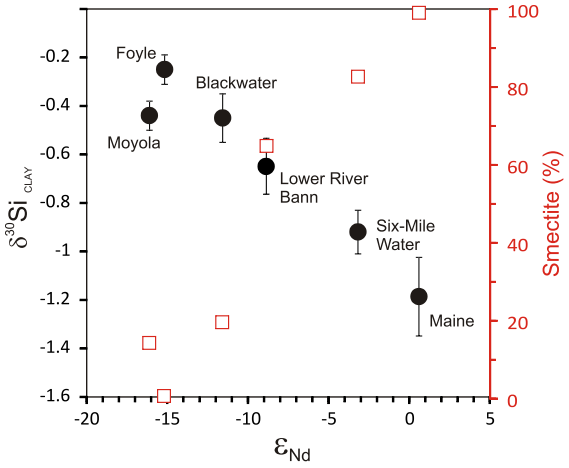

Fig. 7. Relationships between $\delta^{30}Si_{clay}$ (black circles) and corresponding smectite clay mineral proportions (open red squares) function of the corresponding neodymium isotopic composition (ε_{Nd}) in rivers of Northern Ireland. High smectite contents and radiogenic (high) ε_{Nd} values characterize clays derived from the British Tertiary Volcanic province, whereas river material transported from the Paleozoic and Proterozoic terranes display much lower smectite and ε_{Nd} compositions (Bayon et al., 2015).

4.4.2. Congo river basin

4.4.2.1. Influence of sediment recycling. The Congo River and its main tributaries also drain watersheds characterized by roughly similar climatic conditions, but distinct geological settings. Here, the role of lithology was investigated by comparing $\delta^{30}Si_{clay}$ data to the relative proportions of different rock types outcropping in corresponding watersheds (Fig. 8), extracted from the GLiM global lithological map (Hartmann and Moosdorf, 2012). The restricted available quantity of suspended river particulates did not allow us to determine their clay mineralogy. However, information on soil types was provided for each studied river sub-basins using the soil atlas of Africa (Dewitte et al., 2013). All data about lithology and soil types are reported in Table 5. Most of the Congo Basin is covered by ferralsols, which correspond to highly weathered soils dominated by kaolinite, and aluminum and iron oxides. An exception is the southwestern part of the basin, drained by the Kasai River and its tributaries (except for Sankuru), which is dominated by easily erodable quartz-rich sandy soils called arenosols. At the scale of the Congo Basin, no correlation was found between Si isotopes and the nature of soils in studied watersheds (not shown). However, a clear relationship was observed between $\delta^{30}Si_{clay}$ and the lithological composition of corresponding drainage basins (Fig. 8). The river sub-basins exhibiting the heaviest clay $\delta^{30}Si$ suspended sediment compositions host substantial amounts (>80%) of quartz-rich sandy detrital sedimentary rocks covered by quart-rich sandy soils (Lomani, Kasai, Kwango, Loange, Sankuru). In contrast, the rivers displaying the lightest $\delta^{30}Si_{clay}$ values (about $\sim -1.6‰$) correspond to

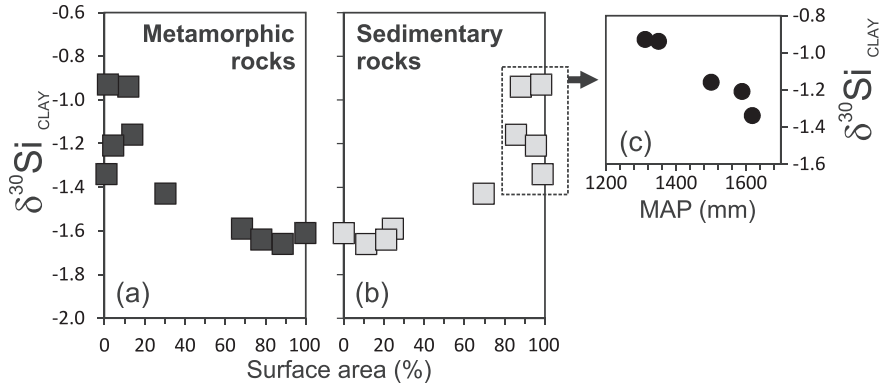

Fig. 8. Relationships between $\delta^{30}Si_{clay}$ and lithology in the Congo River Basin. $\delta^{30}Si_{clay}$ data for suspended particulates from the Congo and Kasai rivers and their main tributaries are reported together with percentage coverage areas of metamorphic (a) and sedimentary (b) rocks in corresponding watersheds. Note that the clay-size fractions from those Congo and Kasai tributaries draining sedimentary basins also display a strong negative correlation with corresponding mean annual precipitation levels (c). The lithological data are derived from the GLiM global lithological map (Hartmann and Moosdorf, 2012).

Table 5
Lithological and soil data (relative surface coverage %) for the studied Congo Basin watersheds.

River	Lithology		Soils							
	Metamorphic rocks	Sedimentary rocks	Acrisols	Arenosols	Cambisols	Ferralsols	Lixisols	Leptisols	Umbrisols	Plinthosols
Lualaba	68.4	24.5	20.7	0.7	18.7	38.0	1.1	4.6	4.1	0.0
Kasai (downstream)	13.9	85.7	5.5	39.4	0.0	49.7	0.7	1.5	0.0	0.0
Ubangui	78.0	21.2	0.1	15.4	0.1	48.5	1.0	0.5	0.0	23.0
Kasai (upstream)	30.3	69.7	2.7	49.2	0.0	46.7	0.0	0.0	0.0	0.0
Sankuru	4.4	95.6	6.3	3.7	0.0	85.6	4.4	0.0	0.0	0.0
Kwango	1.8	98.2	2.3	69.1	0.0	14.2	0.0	7.6	0.0	0.0
Aruwimi	88.7	11.3	0.6	0.0	0.0	59.8	36.9	0.0	0.7	0.0
Lomani	11.9	88.1	20.7	0.0	0.0	79.2	0.0	0.0	0.0	0.0
Loange	1.0	99.0	0.0	71.1	0.0	28.9	0.0	0.0	0.0	0.0
Lindi	99.8	0.2	4.3	0.0	0.0	71.9	22.2	0.0	1.6	0.0

Lithological and soil data are from Hartmann and Moosdorf (2012) and Dewitte et al. (2013), respectively.
Note that only the dominant categories of soils are reported.

watersheds (Lindi, Aruwimi, Ubangui) dominated by metamorphic rocks mostly Archaean in ages (greenstone belts). The light $\delta^{30}Si_{clay}$ signatures of these latter rivers agree well with literature data reported previously for tropical soils developed above crystalline basement rocks in Puerto Rico (Ziegler et al., 2005b). In such settings, intense silicate weathering under warm and humid conditions typically leads to kaolinite formation and development of strongly ^{30}Si-depleted soils. In contrast, one particularity is that those sedimentary formations from the Kasai River Basin include various shales, siltstones, and sandstone deposits of Jurassic and Cretaceous age, which are thought to have formed under semi-arid to arid conditions (Roberts et al., 2015; Owusu et al., 2016), hence characterized by presumably moderately depleted $\delta^{30}Si_{clay}$ signatures. The assumption of low weathering conditions at that time (i.e. during the Jurassic and Cretaceous periods) was inferred from the relative abundance of easily alterable minerals (e.g. plagioclase, pyroxene, amphibole) in these sedimentary formations. Detrital zircon geochronology indicates that these sedimentary formations are mostly derived from the erosion of Archaean and Paleoproterozoic terranes composed of anorthosites, gabbro-nortites and granites, hence possibly involving recycling of substantial amounts of high-temperature hydrothermal illite and chlorite associated with presumably relatively heavy $\delta^{30}Si$ signatures (see discussion Section 4.2). In this context, it is likely that a substantial proportion of fine-grained sediments transported by the Kasai River and its tributaries corresponds to recycled clays with relatively heavy Si isotopic compositions derived from the above-mentioned Mesozoic sedimentary formations. As suggested previously on the basis of major and trace element abundances (Gaillardet et al., 1999b) and Li isotopes (Dellinger et al., 2014), this example from the Congo Basin hence clearly shows that recycling of fine-grained sediments issued from former sedimentary cycles are also likely to play an important role in controlling the distribution of Si isotopes in suspended river particulates.

4.4.2.2. Presence of a modern climatic signature during recycling of old sedimentary rocks?. In addition to our case study from the Congo Basin, the importance of sediment recycling in large river systems has been also inferred from the application of Li isotopes to the suspended load of the Amazon, Mackenzie and Ganga-Bhramaputra rivers (Dellinger et al., 2014). The evidence that recycling of old sedimentary rocks strongly influences the geochemistry of sediments transported in large river basins markedly contrasts with our previous observation that $\delta^{30}Si$ clay for the largest rivers worldwide correlate well with modern climatic parameters (see Section 4.3). Interestingly, when considered separately, the clay-size fractions from those Congo and Kasai tributaries draining sedimentary basins also display a strong negative correlation with corresponding mean annual precipitation levels (Fig. 8c). This observation echoes with results from an earlier investigation of Phanerozoic shales collected along a latitudinal transect in the Appalachian Mountains (NE America), which showed that the degree of shale weathering was still clearly correlated with present-day climatic parameters (Dere et al., 2013). Therefore, in agreement with this latter work, our own results for the Congo River Basin would suggest that Si isotopes can still provide constraints on modern weathering and climatic parameters in sedimentary basins. Importantly, this finding would provide an explanation for the fact that the world's largest river systems, which typically integrate a large diversity of lithologies including sedimentary rocks, still display a strong correlation between $\delta^{30}Si_{clay}$ and present-day climate.

5. CONCLUSIONS AND PERSPECTIVES

The data presented in this study confirm that continental weathering leads to coherent ^{30}Si-depletion in fine-grained sediments and governs the $\delta^{30}Si$ isotopic composition of clay-size fractions transported by rivers. At the basin-scale, the $\delta^{30}Si_{clay}$ signature of river sediments is strongly influenced by various lithological effects, such as the susceptibility of different rock types to weathering and sediment recycling in watersheds that mainly host sedimentary formations. Tectonic setting also plays an important role in controlling the Si isotope composition of river sediments. Sediments exported from high mountain areas dominated by kinetically-limited weathering regimes are associated with less ^{30}Si-depleted isotope signatures compared to those derived from lowlands or flat highland areas, where more intense weathering processes can lead to strongly negative $\delta^{30}Si_{clay}$ compositions. At the global scale, climate represents a major control on the Si isotope composition of river sediments, as inferred from general relationships between $\delta^{30}Si_{clay}$ and the mean annual temperature (MAT) and precipitation (MAP) in corresponding drainage basins. Overall, our findings have implications for the usefulness of Si isotopes as potential paleoenvironmental tracers in future studies. The demonstrated sensitivity of clay-bound Si isotope compositions to climate (especially temperature) and silicate weathering intensity on continents indicates that past climatic fluctuations could be reflected in the $\delta^{30}Si$ sedimentary record of past river discharges. An important pre-requirement prior to further establishing Si isotopes as paleoclimate proxies will be to further investigate their behaviour during early diagenetic processes, especially during reverse weathering that may occur at ocean margin settings, and assess whether or not the $\delta^{30}Si$ weathered signatures initially acquired on continents can be faithfully preserved in sedimentary records.

ACKNOWLEDGMENTS

We gratefully acknowledge all our friends and colleagues who very kindly provided us with the studied samples: O. Adeaga, J. Allard, C. Bigler, F. Busschers, G. Calvès, K. Cohen, P. Debrock, B. Dennielou, F.X. Gingele, D. Haynes, P.R. Hill, B. Hoogendoorn, S. Jorry, G. Kowaleska, T. Leipe, S. Leroy, L. Lopez, J. P. Lunkla, I. Mendes, D. Meunier, C. Nittrouer, A. Pasquini, V. Ponomareva, Y. Saito, E. Schefuss, V. Shevchenko, L. Tiron, D. Toucanne, S. VanLaningham, A. Wheeler. We thank Jens Hartmann for access to the GLiM data-set. The suspended river particulates from the Congo Basin were collected in the frame of the TRANSCONGO project funded by the Belgium Fonds National de la Recherche Scientifique (FNRS; 14711103) and of the European Research Council Starting Grant AFRIVAL (240002). A.V. B. is a senior research associate at the FNRS. This work was funded through an IEF Marie Curie fellowship to G.B. (SI-PALEO; Grant No. FP7-PEOPLE-2012-IEF 327778).

REFERENCES

Abraham K., Opfergelt S., Fripiat F., Cavagna A.-J., De Jong J., Foley S. F., André L. and Cardinal D. (2008) $\delta^{30}Si$ and $\delta^{29}Si$ determinations on USGS BHVO-1 and BHVO-2 reference materials with a new configuration on a Nu plasma multi-collector ICP-MS. *Geostand. Geoanal. Res.* **32**, 193–202.

Ameijeiras-Mariño Y., Opfergelt S., Schoonejans J., Vanacker V., Sonnet P., de Jong J. and Delmelle P. (2017) Impact of low denudation rates on soil chemical weathering intensity: a multiproxy approach. *Chem. Geol.* **456**, 72–84.

André L., Cardinal D., Alleman L. Y. and Moorbath S. (2006) Silicon isotopes in ~3.8 Ga West Greenland rocks as clues to the Eoarchaean supracrustal Si cycle. *Earth Planet. Sci. Lett.* **245**, 162–173.

Bayon G., German C. R., Boella R. M., Milton J. A., Taylor R. N. and Nesbitt R. W. (2002) An improved method for extracting marine sediment fractions and its application to Sr and Nd isotopic analysis. *Chem. Geol.* **187**, 179–199.

Bayon G., Barrat J. A., Etoubleau J., Benoit M., Bollinger C. and Revillon S. (2009) Determination of Rare Earth Elements, Sc, Y, Zr, Ba, Hf and Th in Geological Samples by ICP-MS after Tm Addition and Alkaline Fusion. *Geostand. Geoanal. Res.* **33**, 51–62.

Bayon G., Toucanne S., Skonieczny C., André L., Bermell S., Cheron S., Dennielou B., Etoubleau J., Freslon N., Gauchery T., Germain Y., Jorry S. J., Ménot G., Monin L., Ponzevera E., Rouget M. L., Tachikawa K. and Barrat J. A. (2015) Rare earth elements and neodymium isotopes in world river sediments revisited. *Geochim. Cosmochim. Acta* **170**, 17–38.

Bayon G., Skonieczny C., Delvigne C., Toucanne S., Bermell S., Ponzevera E. and André L. (2016) Environmental Hf-Nd isotopic decoupling in World river clays. *Earth Planet. Sci. Lett.* **438**, 25–36.

Bern C. R., Brzezinski M. A., Beucher C., Ziegler K. and Chadwick O. A. (2010) Weathering, dust, and biocycling effects

on soil silicon isotope ratios. *Geochim. Cosmochim. Acta* **74**, 876–889.

Cardinal D., Gaillardet J., Hughes H. J., Opfergelt S. and Andre L. (2010) Contrasting silicon isotope signatures in rivers from the Congo Basin and the specific behaviour of organic-rich waters. *Geophys. Res. Lett.* **37**(L12403), 21.

Cockerton H. E., Street-Perrott F. A., Leng M. J., Barker P. A., Horstwood M. S. A. and Pashley V. (2013) Stable-isotope (H, O, and Si) evidence for seasonal variations in hydrology and Si cycling from modern waters in the Nile Basin: implications for interpreting the Quaternary record. *Quat. Sci. Rev.* **66**, 4–21.

Cornelis J. T., Delvaux B., Cardinal D., Andre L., Ranger J. and Opfergelt S. (2010) Tracing mechanisms controlling the release of dissolved silicon in forest soil solutions using Si isotopes and Ge/Si ratios. *Geochim. Cosmochim. Acta* **74**, 3913–3924.

Cornelis J. T., Weis D., Lavkulich L., Vermeire M. L., Delvaux B. and Barling J. (2014) Silicon isotopes record dissolution and re-precipitation of pedogenic clay minerals in a podzolic soil chronosequence. *Geoderma* **235**, 19–29.

De la Rocha C. L., Brzezinski M. A. and DeNiro M. J. (2000) A first look at the distribution of the stable isotopes of silicon in natural waters. *Geochim. Cosmochim. Acta* **64**, 2467–2477.

Dellinger M., Gaillardet J., Bouchez J., Calmels D., Galy V., Hilton R. G., Louvat P. and France-Lanord C. (2014) Lithium isotopes in large rivers reveal the cannibalistic nature of modern continental weathering and erosion. *Earth Planet. Sci. Lett.* **401**, 359–372.

Delstanche S., Opfergelt S., Cardinal D., Elsass F., André L. and Delvaux B. (2009) Silicon isotopic fractionation during adsorption of aqueous monosilicic acid onto iron oxide. *Geochim. Cosmochim. Acta* **73**, 923–934.

Delvigne C., Opfergelt S., Cardinal D., Hofmann A. and André L. (2016) Desilication in Archean weathering processes traced by silicon isotopes and Ge/Si ratios. *Chem. Geol.* **420**, 139–147.

Dempster M., Dunlop P., Scheib A. and Cooper M. (2013) Principal component analysis of the geochemistry of soil developed on till in Northern Ireland. *J. Maps* **9**, 373–389.

Dere A. L., White T. S., April R. H., Reynolds B., Miller T. E., Knapp E. P., McKay L. D. and Brantley S. L. (2013) Climate dependence of feldspar weathering in shale soils along a latitudinal gradient. *Geochim. Cosmochim. Acta* **122**, 101–126.

Dessert C., Dupré B., Gaillardet J., François L. M. and Allègre C. J. (2003) Basalt weathering laws and the impact of basalt weathering on the global carbon cycle. *Chem. Geol.* **202**, 257–273.

Dewitte O., Jones A., Spaargaren O., Breuning-Madsen H., Brossard M., Dampha A., Deckers J., Gallali T., Hallett S., Jones R., Kilasara M., Le Roux P., Michéli E., Montanarella L., Thiombiano L., Van Ranst E., Yemefack M. and Zougmore R. (2013) Harmonisation of the soil map of Africa at the continental scale. *Geoderma* **211–212**, 138–153.

Ding T., Jiang S., Wan D., Li Y., Li J., Song H., Liu Z. and Yao X. (1996) *Silicon Isotope Geochemistry*. Geological Publishing House, Beijing, China.

Ding T., Wan D., Wang C. and Zhang F. (2004) Silicon isotope compositions of dissolved silicon and suspended matter in the Yangtze River China. *Geochim. Cosmochim. Acta* **68**, 205–216.

Douthitt C. B. (1982) The geochemistry of the stable isotopes of silicon. *Geochim. Cosmochim. Acta* **46**, 1449–1458.

Edmond J. M., Palmer M. R., Measures C. I., Grant B. and Stallard R. F. (1995) The fluvial geochemistry and denudation rate of the Guayana Shield in Venezuela, Colombia, and Brazil. *Geochim. Cosmochim. Acta* **59**, 3301–3325.

Edmond J. M. and Huh Y. (1997) Chemical weathering yields in hot and cold climates. In: Tectonic Uplift and Climate Change, Ruddiman W. F. (Ed.), Plenum, New York, pp. 558.

Frings P. J., Clymans W., Fontorbe G., De La Rocha C. L. and Conley D. J. (2016) The continental Si cycle and its impact on the ocean Si isotope budget. *Chem. Geol.* **425**, 12–36.

Gaillardet J., Dupré B., Louvat P. and Allègre C. J. (1999a) Global silicate weathering and CO_2 consumption rates deduced from the chemistry of large rivers. *Chem. Geol.* **159**, 3–30.

Gaillardet J., Dupré B. and Allègre C. J. (1999b) Geochemistry of large river suspended sediments: silicate weathering or recycling tracer? *Geochim. Cosmochim. Acta* **63**, 4037–4051.

Georg R. B., Reynolds B. C., Frank M. and Halliday A. N. (2006a) Mechanisms controlling the silicon isotopic compositions of river waters. *Earth Planet. Sci. Lett.* **249**, 290–306.

Georg R. B., Reynolds B. C., Frank M. and Halliday A. N. (2006b) New sample preparation techniques for the determination of Si isotopic compositions using MC-ICPMS. *Chem. Geol.* **235**, 95–104.

Georg R. B., Reynolds B. C., West A. J., Burton K. W. and Halliday A. N. (2007) Silicon isotope variations accompanying basalt weathering in Iceland. *Earth Planet. Sci. Lett.* **261**, 476–490.

Georg R. B., Zhu C., Reynolds B. C. and Halliday A. N. (2009) Stable silicon isotopes of groundwater, feldspars, and clay coatings in the Navajo Sandstone aquifer, Black Mesa, Arizona, USA. *Geochim. Cosmochim. Acta* **73**, 2229–2241.

Gingele F. X. and De Deckker P. (2004) Fingerprinting Australia's rivers with clay minerals and the application for the marine record of climate change. *Austral. J. Earth Sci.* **51**, 339–348.

Goldstein S. L. and Hemming S. R. (2003) Long-lived Isotopic Tracers in Oceanography, Paleoceanography, and Ice-sheet Dynamics. In: Treatise on Geochemistry, vol. 6, 453-489, Elderfield H. (Ed.), Holland H. D. and Turekian K. T. (Exec. Eds.), Elsevier-Pergamon, Oxford, pp. 625.

Hartmann J. and Moosdorf M. (2012) The new global lithological map database GLiM: a representation of rock properties at the Earth surface. *Geochem. Geophys. Geosyst.* **13**, Q12004. https://doi.org/10.1029/2012GC004370.

Hughes H. H., Delvigne C., Korntheuer M., De Jong J., André L. and Cardinal D. (2011) Controlling the mass bias introduced by anionic and organic matrices in silicon isotopic measurements by MC-ICP-MS. *J. Anal. Atom. Spectrom.* **26**, 1892–1896.

Hughes H. H., Sondag F., Santos R. V., André L. and Cardinal D. (2013) The riverine silicon isotope composition of the Amazon Basin. *Geochim. Cosmochim. Acta* **121**, 637–651.

Méheut M., Lazzeri M., Balan E. and Mauri F. (2007) Equilibrium isotopic fractionation in the kaolinite, quartz, water system: prediction from first-principles density-functional theory. *Geochim. Cosmochim. Acta* **71**, 3170–3181.

Méheut M., Lazzeri M., Balan E. and Mauri F. (2009) Structural control over equilibrium silicon and oxygen isotopic fractionation: a first-principles density-functional theory study. *Chem. Geol.* **258**, 28–37.

Méheut M. and Schauble E. A. (2014) Silicon isotope fractionation in silicate minerals: insights from first-principles models of phyllosilicates, albite and pyrope. *Geochim. Cosmochim. Acta* **134**, 137–154.

Michalopoulos P. and Aller R. C. (1995) Rapid Clay Mineral formation in amazon delta sediments – reverse weathering and oceanic elemental cycles. *Science* **270**, 614–617.

Milliman J. D. and Farnsworth K. L. (2011) *River Discharge to the Coastal Ocean*. Cambridge University Press, A global synthesis, p. 392.

Milliman J. D. and Syvitski J. P. M. (1992) Geomorphic/tectonic control of sediment discharge to the ocean: the importance of small mountainous rivers. *J. Geol.* **100**, 525–544.

Oelze M., von Blanckenburg F., Hoellen D., Dietzel M. and Bouchez J. (2014) Si stable isotope fractionation during

adsorption and the competition between kinetic and equilibrium isotope fractionation: Implications for weathering systems. *Chem. Geol.* **380**, 161–171.

Oelze M., von Blanckenburg F., Bouchez J., Hoellen D. and Dietzel M. (2015) The effect of Al on Si isotope fractionation investigated by silica precipitation experiments. *Chem. Geol.* **397**, 94–105.

Opfergelt S. and Delmelle P. (2012) Silicon isotopes and continental weathering processes: assessing controls on Si transfer to the ocean. *C. R. Geosci.* **344**, 723–738.

Opfergelt S., Cardinal D., André L., Delvigne C., Bremond L. and Delvaux B. (2010) Variation of δ^{30}Si and Ge/Si with weathering and biogenic input in tropical basaltic ash soils under monoculture. *Geochim. Cosmochim. Acta* **74**, 225–240.

Opfergelt S., Georg R. B., Delvaux B., Cabidoche Y.-M., Burton K. W. and Halliday A. N. (2012) Silicon isotopes and the tracing of desilication in volcanic soil weathering sequences, Guadeloupe. *Chem. Geol.* **326–327**, 113–122.

Opfergelt S., Williams H. M., Cornelis J.-T., Guicharnaud R. A., Georg R. B., Siebert C., Gislason S. R., Halliday A. N. and Burton K. W. (2017) Iron and silicon isotope behaviour accompanying weathering in Icelandic soils, and the implications for iron export from peatlands. *Geochim. Cosmochim. Acta* **217**, 273–291.

Owusu Agyemang P. C., Roberts E. M. and Jelsma H. A. (2016) Late Jurassic-Cretaceous fluvial evolution of central Africa: Insights from the Kasai-Congo Basin, Democratic Republic Congo. *Cretac. Res.* **67**, 25–43.

Pogge von Strandmann P. A. E., Opfergelt S., Lai Y. J., Sigfússon B., Gislason S. R. and Burton K. W. (2012) Lithium, magnesium and silicon isotope behaviour accompanying weathering in a basaltic soil and pore water profile in Iceland. *Earth Planet. Sci. Lett.* **339**, 11–23.

Pokrovsky O. S., Reynolds B. C., Prokushkin A. S., Schott J. and Viers J. (2013) Silicon isotope variations in Central Siberian rivers during basalt weathering in permafrost-dominated larch forests. *Chem. Geol.* **355**, 103–116.

Poitrasson F. (2017) Silicon isotope geochemistry. *Rev. Mineral. Geochem.* **82**, 289–344.

Reynolds B. C., Aggarwal J., Andre L., Baxter D., Beucher C., Brzezinski M. A., Engström E., Georg R. B., Land M., Leng M. J., Opfergelt S., Rodushkin I., Sloane H. J., van den Boorn S. H. J. M., Vroon P. Z. and Cardinal D. (2007) An inter-laboratory comparison of Si isotope reference materials. *J. Anal. Atom. Spectrom.* **22**, 561–568.

Roberts E., Jelsma H. A. and Hegna T. (2015) Mesozoic Sedimentary Cover Sequences of the Congo Basin in the Kasai Region, Democratic Republic of Congo. In: Geology and Resource Potential of the Congo Basin, 163-191, de Wit M. J., Guillocheau F. and de Wit M. C. J. (Eds.), Springer-Verlag Berlin Heidelberg, doi:10.1007/978-3-642-29482-2_9.

Rudnick R. L. and Gao S. (2003) The Composition of the Continental Crust. In: Treatise on Geochemistry, vol. 3, 1–64, Rudnick R. L. (Ed.), Holland H. D. and Turekian K. T. (Exec. Eds.), Elsevier-Pergamon, Oxford, pp. 625.

Savage P. S., Georg R. B., Armytage R. M. G., Williams H. M. and Halliday A. N. (2010) Silicon isotope homogeneity in the mantle. *Earth Planet. Sci. Lett.* **295**, 139–146.

Savage P. S., Georg R. B., Williams H. M., Turner S., Halliday A. N. and Chappell B. W. (2012) The silicon isotope composition of granites. *Geochim. Cosmochim. Acta* **92**, 184–202.

Savage P. S., Georg R. B., Williams H. M. and Halliday A. N. (2013) The silicon isotope composition of the upper continental crust. *Geochim. Cosmochim. Acta* **109**, 384–399.

Steinhoefel G., Breuer J., von Blanckenburg F., Horn I., Kaczorek D. and Sommer M. (2011) Micrometer silicon isotope diagnostics of soils by UV femtosecond laser ablation. *Chem. Geol.* **286**, 280–289.

Steinhoefel G., Breuer J., von Blanckenburg F., Horn I. and Sommer M. (2017) The dynamics of Si cycling during weathering in two small catchments in the Black Forest (Germany) traced by Si isotopes. *Chem. Geol.* **466**, 389–402.

Vandevenne F. I., Delvaux C., Hughes H. J., André L., Ronchi B., Clymans W., Barao L., Cornelis J. T., Govers G., Meire P. and Struyf E. (2015) Landscape cultivation alters δ^{30}Si signature in terrestrial ecosystems. *Sci. Rep.* **5**, 7732.

West A. J., Galy A. and Bickle M. (2005) Tectonic and climatic control on silicate weathering. *Earth Planet. Sci. Lett.* **235**, 211–228.

White A. F. and Blum A. E. (1995) Effects of climate on chemical weathering rates in watersheds. *Geochim. Cosmochim. Acta* **59**, 1729–1747.

White A. F., Blum A. E., Bullen T. D., Vivit D. V., Schulz M. and Fitzpatrick J. (1999) The effect of temperature on experimental and natural chemical weathering rates of granitoid rocks. *Geochim. Cosmochim. Acta* **63**, 3277–3291.

Ziegler K., Chadwick O. A., Brzezinski M. A. and Kelly E. F. (2005a) Natural variations of delta Si-30 ratios during progressive basalt weathering, Hawaiian Islands. *Geochim. Cosmochim. Acta* **69**, 4597–4610.

Ziegler K., Chadwick O. A., White A. F. and Brzezinski M. A. (2005b) (DSi)-Si-30 systematics in a granitic saprolite, Puerto Rico. *Geology* **33**, 817–820.

Associate editor: Fang-Zhen Teng